The Holocene 15,7 (2005) pp. 951–964

Holocene climate evolution in the high-latitude Southern Hemisphere simulated by a coupled atmosphere–sea ice–ocean–vegetation model

Hans Renssen,[1*] Hugues Goosse,[2] Thierry Fichefet,[2] Valérie Masson-Delmotte[3] and Nalan Koç[4]

([1]Faculty of Earth and Life Sciences, Vrije Universiteit Amsterdam, De Boelelaan 1085, NL-1081 HV, The Netherlands; [2]Institut d'Astronomie et de Géophysique Georges Lemaître, Université catholique de Louvain, Chemin du Cyclotron 2, B-1348 Louvain-la-Neuve, Belgium; [3]Laboratoire des Sciences du Climat et de l'Environment, IPSL/CEA-CNRS, F-19 191 Gif sur Yvette cedex, France; [4]Norwegian Polar Institute, the Polar Environmental Center, N-9296 Tromsø, Norway)

Received 7 November 2004; revised manuscript accepted 22 April 2005

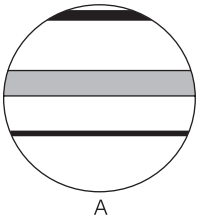

Abstract: The Holocene climate is simulated in a 9000-yr-long transient experiment performed with the ECBilt-CLIO-VECODE coupled atmosphere–sea ice–ocean–vegetation model. This experiment is forced with annually varying orbital parameters and atmospheric concentrations of CO_2 and CH_4. The objective is to study the impact of these long-term forcings on the surface temperature evolution during different seasons in the high-latitude Southern Hemisphere. We find in summer a thermal optimum in the mid-Holocene (6–3 ka BP), with temperatures locally 3°C above the preindustrial mean. In autumn the temperatures experienced a long-term increase, particularly during the first few thousand years. The opposite trend was simulated for winter and spring, with a relatively warm Southern Ocean at 9 ka BP in winter (up to 3.5°C above the preindustrial mean) and a warm continent in spring (+3°C), followed by a gradual cooling towards the present. These long-term temperature trends can be explained by a combination of (1) a delayed response to orbital forcing, with temperatures lagging insolation by 1 to 2 months owing to the thermal inertia of the system, and (2) the long memory of the Southern Ocean. This long memory is related to the storage of the warm late winter–spring anomaly below the shallower summer mixed layer until next winter. Sea ice plays an important role as an amplifying factor through the ice–albedo and ice–insulation feedbacks. Our experiments can help to improve our understanding of the Holocene signal in proxies. For instance, the results suggest that, in contrast to recent propositions, teleconnections to the Northern Hemisphere appear not necessarily to explain the history of Southern Hemisphere temperature changes during the Holocene.

Key words: Climate model simulation, coupled model, climate change, Southern Hemisphere, teleconnections, Southern Ocean, Antarctica, orbital forcing, Holocene.

Introduction

Over the past few decades, the high-latitude Southern Hemisphere (SH) climate has experienced significant changes (e.g., Folland *et al*., 2001; Thompson and Solomon, 2002). The character of these climatic changes is complex, as the trends appear to be disparate at different locations. For instance, the limited data available suggest that in recent decades temperatures over the Antarctic Peninsula have increased (Folland *et al*., 2001; Vaughan *et al*., 2001), while a small cooling was noted over the Antarctic interior. Similarly, sea ice concentrations have decreased in some areas (e.g., Bellingshausen Sea; Jacobsen and Comiso, 1997), while the sea ice extent has increased elsewhere (e.g., Eastern Antarctica, Ross Sea; Stammerjohn and Smith, 1997). The sparse network of

*Author for correspondence (e-mail: hans.renssen@geo.falw.vu.nl)

10.1191/0959683605hl869ra

observations and the limited length of the measured time series seriously hamper the analysis of these recent changes. Yet, considering the major climate changes that are projected to occur at SH high latitudes in the near future, under the influence of anthropogenic forcing (Cubasch *et al*., 2001), then it is important to improve our understanding of the mechanisms governing these changes. An essential step is to gain more insight into the natural climate variability at different timescales. From this perspective, it is important to study the long-term natural climate variations that have occurred during the Holocene.

Compared with the Northern Hemisphere, only a few proxy-based reconstructions of the Holocene climatic evolution are available for the SH high latitudes. These reconstructions all show a Holocene thermal optimum, with temperatures well above the present-day levels. However, the timing and character of this optimum varies considerably from place to place. For example, an analysis of 11 Antarctic ice cores by Masson *et al.* (2000) revealed an early Holocene thermal optimum between 11.5 and 9 ka (thousand calendar years before present), followed by a relatively cool period and a secondary optimum that varied in timing between 7–5 ka (Ross Sea sector) and 6–3 ka (Eastern Antarctica). Other records (marine, lacustrine) confirm the complexity of the Holocene temperature evolution around Antarctica, as maximum warming was registered between 12 and 7 ka in the Atlantic sector (Nielsen *et al*., 2004), but between 9 and 4 ka in the area of Antarctic Peninsula (Domack *et al*., 2001; Brachfeld *et al*., 2003), and 5 and 3 ka at the East Antarctic coast (Verkulich *et al*., 2002). The proxy data thus suggest considerable latitudinal and longitudinal thermal gradients at SH high latitudes. However, the processes that are responsible for these gradients have not yet been identified.

The main external forcing driving Holocene climate changes are variations in orbital parameters. A thermal optimum early in the Holocene is consistent with orbital forcing, as south of 43°S the received sum of annual insolation was slightly higher at 9 ka than today, with the amplitude increasing towards the South Pole (Berger, 1978). For instance, compared with today, the surplus annual insolation at 9 ka was 1 W/m^2 at 60°S and 5 W/m^2 at 80°S. During the course of the Holocene, the annual insolation gradually decreased towards the present-day values. However, the seasonal patterns of insolation are more complex, as the early Holocene insolation at SH high latitudes was only higher than present in late winter–spring (August to November, maximum difference at 60°S of +36 W/m^2 in October), while it was lower than today in summer (December to March, minimum at 60°S of −31 W/m^2 in January). During most of the autumn and winter (i.e., from April to July), the Holocene changes in insolation were very small at SH high latitudes. To complicate matters further, during November and December the difference in insolation at 60°S reached an optimum at 6 ka (+22 W/m^2) and 3 ka (+5 W/m^2), respectively.

In addition to orbital forcing, changes in the atmospheric concentration of greenhouse gases could also have played a role in driving long-term climate changes at high SH latitudes. The concentration of CO_2 increased steadily by 20 ppm from ∼260 ppm at 9 ka to ∼280 ppm at preindustrial times, whereas the global mean CH_4 content first decreased from ∼660 ppb at 9 ka to ∼580 ppb at 5 ka and then increased towards a preindustrial value of ∼710 ppb (Raynaud *et al*., 2000). These increases in atmospheric CO_2 and CH_4 concentrations correspond approximately to radiative forcings of 0.4 W/m^2 and 0.1 W/m^2, respectively.

In the palaeoclimatic literature, various relationships between insolation and climate at SH high latitudes have been proposed. Some researchers have related Holocene climate evolution, as reconstructed from proxy data (i.e., relatively warm early to mid Holocene, followed by cooling in the late Holocene), to the response to summer insolation changes at northern high latitudes. For instance, Hodell *et al.* (2001) find relatively warm conditions in the Atlantic sector of the Southern Ocean in the early Holocene (before 5.5 ka), which they link to a relatively weak ocean thermohaline circulation under the influence of summer insolation at 65°N. This could have led to reduced northward Atlantic Ocean heat transport and accumulation of heat in the Southern Ocean. Similarly, Nielsen *et al.* (2004) found in an ocean core in the same region a Holocene climate optimum that is followed by a 3°C summer cooling and expansion of sea ice, which is also explained as a response to the summer insolation at Northern Hemisphere high latitudes. Others have suggested that changes in SH insolation drive observed variations in proxy records covering the Holocene. For example, the Holocene trend observed in Antarctic deuterium excess records (i.e., increase during the first half of the Holocene) has been associated with a reduced efficiency of the low-to-high latitude atmospheric moisture transport in response to the decreasing annual mean meridional SH insolation gradient (Vimeux *et al*., 2001). Lamy *et al.* (2002), on the other hand, related the decrease in Holocene temperature (after 6 ka) in the Peru–Chile current at 40°S to a reduction in the seasonal difference in insolation.

Our insight into the response of the climate system to long-term Holocene changes in forcing may be improved with the aid of numerical climate models (Weber, 2001; Crucifix *et al*., 2002; Brovkin *et al*., 2002; Weber *et al*., 2004; Wang *et al*., 2005). Model studies have, for instance, shown that the surface temperatures at SH high latitudes experienced a 1–2 month lag compared with orbital forcing (e.g., Hewitt and Mitchell, 1998). However, so far, modelling studies have not focused on the longer-term scale of Holocene climate evolution in the SH high latitudes, partly because of the relatively poor representation of the Southern Ocean in the applied models. We therefore present here the results of a transient Holocene experiment performed with a coupled global atmosphere–sea ice–ocean–vegetation model that simulates a reasonable modern climate in the SH high latitudes, including the dynamics in the Southern Ocean (Goosse and Renssen, 2001, 2005; Goosse *et al*., 2004). Our experiment covers the last 9 000 years and was forced by variations in orbital parameters and atmospheric concentrations of CO_2 and CH_4. Our main objective is to unravel the long-term response to these main forcings. We focus on the surface temperature evolution, as the main climatic parameter reconstructed from proxy records. First, we discuss the long-term trends of simulated SH climate parameters and, secondly, we analyse the spatial patterns of the 9–0 and 4.5–0 ka anomalies.

Model and experimental design

We have performed our experiment with version 3 of the global, three-dimensional intermediate complexity climate model ECBilt-CLIO-VECODE. The atmospheric module ECBilt is a spectral quasi-geostrophic model with three levels and T21 resolution (Opsteegh *et al*., 1998), which includes a representation of the hydrological cycle and simple parameterizations of the diabatic heating processes. Cloudiness is prescribed following present-day climatology (Rossow *et al*., 1996) and a dynamically passive stratospheric layer is incorporated.

As an extension to the quasi-geostrophic equations, an estimate of the neglected terms in the vorticity and thermodynamic equations is included as a temporally and spatially varying forcing. This forcing is calculated from the diagnostically derived vertical motion field and leads to a considerable improvement of the simulation of the Hadley Cell circulation, resulting in a better representation of the strength and position of the jet stream and transient eddy activity. Weber (2001) and Weber *et al.* (2004) have studied the climate response to insolation forcing in experiments performed with this atmospheric component ECBilt coupled to a flat-bottom ocean model.

We have applied a model version in which ECBilt is coupled to CLIO, a primitive-equation, free-surface oceanic general circulation model coupled to a thermodynamic-dynamic sea ice model (Goosse and Fichefet, 1999). The ocean model includes a detailed formulation of boundary layer mixing based on Mellor and Yamada's (1982) level -2.5 turbulence closure scheme (Goosse *et al.*, 1999) and a parameterization of density-driven downslope flows (Campin and Goosse, 1999). The sea ice model takes into account the heat capacity of the snow–ice system, the storage of latent heat in brine pockets trapped inside the ice, the effect of the subgrid-scale snow and ice thickness distributions on sea ice thermodynamics, the formation of snow ice under excessive snow loading and the existence of leads within the ice cover. Ice dynamics are computed by assuming that sea ice behaves as a two-dimensional viscous-plastic continuum. The horizontal resolution of CLIO is 3° latitude by 3° longitude, and there are 20 unequally spaced levels in the vertical.

Version 3 of ECBilt-CLIO model was recently applied by Knutti *et al.* (2004) to study the impact of freshwater discharges on the climate during the last glacial stage. It is an improved and updated version of the model applied previously (i.e., version 2) to simulate the modern climate and its natural variability (Goosse *et al.*, 2001, 2002, 2003; Goosse and Renssen, 2004), and to study the 8.2 ka event (Renssen *et al.*, 2001, 2002) and the future climate evolution (Goosse and Renssen, 2001; Schaeffer *et al.*, 2002). The most important improvements in version 3 of ECBilt-CLIO are a new land surface scheme that accounts for soil heat capacity, and the utilization of isopycnal diffusion as well as Gent and McWilliams parameterization to represent the effect of meso-scale eddies in the ocean (Gent and McWilliams, 1990). The climate sensitivity of ECBilt-CLIO is in the order of $0.5°C/(W/m^2)$, which is at the lower end of the range found in most coupled climate models (Cubasch *et al.*, 2001). The only flux correction required in ECBilt-CLIO is an artificial reduction of precipitation over the Atlantic and Arctic oceans, and a homogeneous distribution of this removed amount of freshwater over the Pacific Ocean (Goosse *et al.*, 2001).

Recently, ECBilt-CLIO3 has been coupled to VECODE, a global vegetation model (Brovkin *et al.*, 2002) that simulates the dynamics of two main terrestrial plant functional types, trees and grasses, as well as desert (bare soil), in response to climate change. Within ECBilt-CLIO-VECODE, simulated vegetation changes only have an impact on the land-surface albedo, and have no influence on other processes, e.g., evapotranspiration (Renssen *et al.*, 2003a,b).

Our main experiment is a 9000-yr transient simulation that was forced by annually varying insolation values (Figure 1a, Berger, 1978) and smoothed time series for atmospheric concentrations of CH_4 and CO_2 (Figure 1b, Raynaud *et al.*, 2000). Concerning the calendar employed, it should be noted

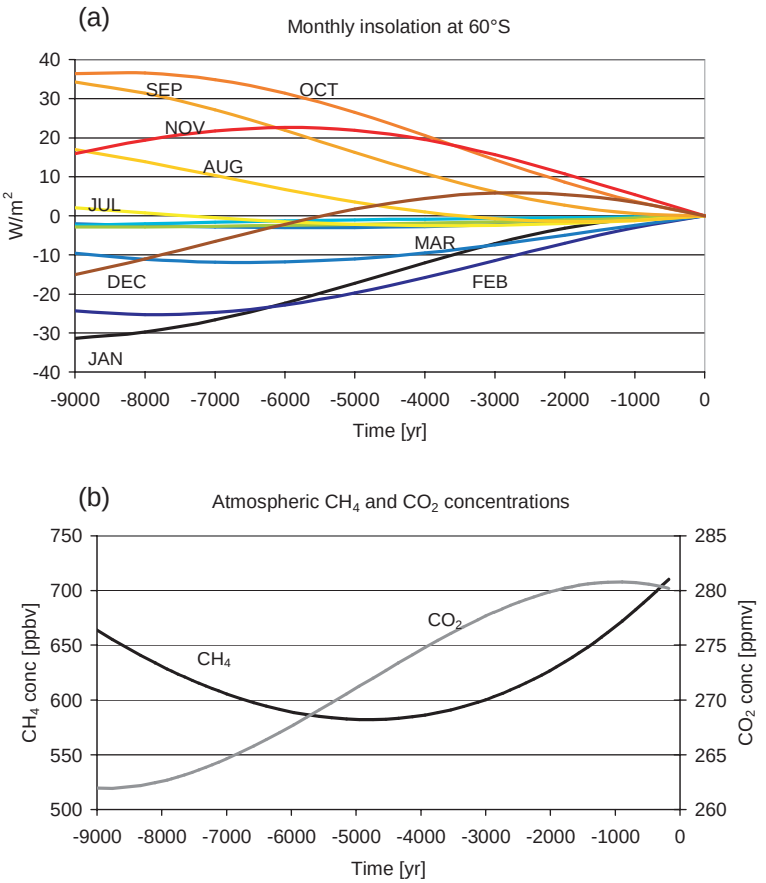

Figure 1 Variations in external forcing. (a) Monthly insolation at 60°S over the last 9000 years (Berger, 1978) plotted as deviation from the present-day mean. (b) Long-term smoothed trends of the atmospheric concentrations of CO_2 and CH_4, based on ice core measurements (Raynaud *et al.*, 2000)

that we fixed the vernal equinox at day 81, while in our model one year is divided into 12 months of 30 days each. This is common practice in modelling studies focusing on Holocene climate (e.g., Crucifix *et al*., 2002; Weber *et al*., 2004). We realize that it would have been more appropriate to use a calendar in which the duration of the months depends on their angular length (Joussaume and Braconnot, 1997) but, as this would require substantial adjustments to our model, we have chosen to apply a calendar with months of equal duration for convenience. All other forcings (i.e., solar constant, other greenhouse gases, ice-sheet configuration) were fixed at their AD 1750 values. Consequently, the impact of ice-volume changes on climate was not taken into account in this experiment. In an earlier paper, we have presented the results for the Northern Hemisphere high latitudes (Renssen *et al*., 2005). We also discuss here some results of a second 9000-yr-long experiment in which we only prescribed the changes in atmospheric content of CH_4 and CO_2, while keeping the orbital parameters fixed at their values for 0 ka. This second simulation is a sensitivity experiment that is used to separate in our model the effects of orbital and greenhouse gas forcing during the Holocene.

The initial conditions for the experiments were derived from equilibrium simulations that were run with constant forcings for 9 ka (i.e., either with both orbital parameters and greenhouse gas concentrations for the main experiment or only the latter forcing for the 'greenhouse only' simulation). Consequently, our experiments do not account for the effect of the long-term (i.e., centennial-to-millennial scale) memory for events that occurred before 9 ka, which could potentially influence the first 1000 years of our simulation (e.g., through the deep ocean). We assume here that this 'memory' effect is negligible.

Results

Surface temperature

Summer

The simulated January temperatures averaged over the area south of 60°S reveal a clear mid-Holocene thermal optimum during summer. The January temperatures gradually increase from +0.5°C above the preindustrial mean at 9 ka to +1.3°C between 6 and 3 ka, after which a relatively rapid cooling sets in towards the present (Figure 2a). This 1.3°C cooling is of the same order as the interannual variability, as expressed by the monthly standard deviation (Table 1). The 9 ka minus 0 ka anomaly map (Figure 3a) suggests a patchy pattern for the early Holocene, with cooler conditions than present along the east coast of Antarctica (max −0.5°C), and warmer conditions elsewhere, most notably in West Antarctica (up to +1.5°C). The January map for the mid-Holocene (4.5 ka minus 0 ka, Figure 4a) gives a view of the thermal conditions during the thermal optimum, with temperatures being more than 3.5°C above the preindustrial level over West Antarctica. The Southern Ocean is between 0.5 and 1°C warmer in January at 4.5 ka.

Autumn

Autumn is the only season showing an increase in the long-term temperature trend throughout the experiment. The total increase in April temperatures south of 60°S is about 0.7°C from 9 to 0 ka (Figure 2a), which is smaller than the standard deviation for April (0.8°C, Table 1). The 9 ka minus 0 ka map for April (Figure 3b) reveals a more complex picture, with the continent being up to 1.5°C cooler at 9 ka than at 0 ka (East Antarctica being the coldest region), but relatively warm conditions over most of the Southern Ocean, particularly over the Bellingshausen Sea (locally +1°C). The map for the mid-Holocene (Figure 4b) shows that at 4.5 ka Eastern Antarctica was still 1°C cooler in the simulation than the preindustrial climate.

Winter

Averaged over the entire study area (i.e., south of 60°S), the simulated July temperatures decreased throughout the Holocene (1.3°C total cooling, Figure 2a), with the main part of the cooling between 9 and 5 ka. This long-term cooling is slightly above the level of the interannual variability, as the monthly standard deviation for July is 1.0°C (Table 1). The anomaly maps indicate that this response is mainly coming from the ocean surface, as the continental temperature evolution shows a different behaviour. The 9 ka temperatures are more than 3.5°C higher than 0 ka over the Southern Ocean along 65°S, with two centres at 90°E and 15°W (Figure 3c). At 4.5 ka, the winter temperatures over the Southern Ocean were still up to 1°C warmer than today. In contrast, temperatures over the continent decrease by 1°C from 9 to 4.5 ka, with the 9 ka conditions being about 0.5°C warmer than 0 ka, while at 4.5 ka they were 0.5°C cooler (compare Figures 3c and 4c). From 4.5 to 0 ka, continental winter temperatures again increase, thus revealing a mid-Holocene thermal minimum.

Spring

In spring the region experiences a relatively strong cooling, with the October temperatures being more than 2.5°C higher at 9 ka than at 0 ka (Figure 2a). This cooling is large compared to the interannual variability, as the standard deviation for October is 0.9°C (Table 1). The 9 ka minus 0 ka map (Figure 3d) shows that this cooling is centred on the continent, where the temperatures are between 2.5°C and 3.5°C higher at 9 ka compared with 0 ka. Over the sea ice cover, the 9 ka minus 0 ka difference is between 2 and 3°C, while the 9 ka minus 0 ka anomaly becomes rapidly smaller over the open ocean (about 0.5°C). The anomaly map for 4.5 ka (Figure 4d) reveals that a substantial part of the Holocene cooling during spring takes place during the last few millennia, as even at 4.5 ka the October temperatures are up to 2.5°C above the preindustrial level.

Annual

Averaged over the area South of 60°S, the annual mean temperatures experience an almost linear 1°C decrease from 9 to 0 ka (not shown). The strongest cooling (more than 1.5°C) occurs over the Bellingshausen Sea between 70 and 120°W and over the Atlantic sector of the Southern Ocean between 0 and 30°E (i.e., same spots as on winter map, Figure 3e). Over the Antarctic continent, the cooling varies between 1°C in west Antarctica and less than 0.5°C on east Antarctica. Thus, when considering the annual mean conditions, western Antarctica experiences a stronger cooling than the eastern part of the continent. This gradient remains present at 4.5 ka (Figure 4e).

Precipitation

The simulated precipitation evolution shows marked differences between seasons, whereby, as expected, precipitation generally follows the temperature trends (Figure 2b). The January time series show more or less stable precipitation levels from 9 to 5 ka, followed by a small decrease of 1 mm. In April, precipitation increases during the course of the experiment (1 mm in total), most notably between 5 and 2 ka. The July time series indicate a 1.6 mm decrease from 9 to 0 ka.

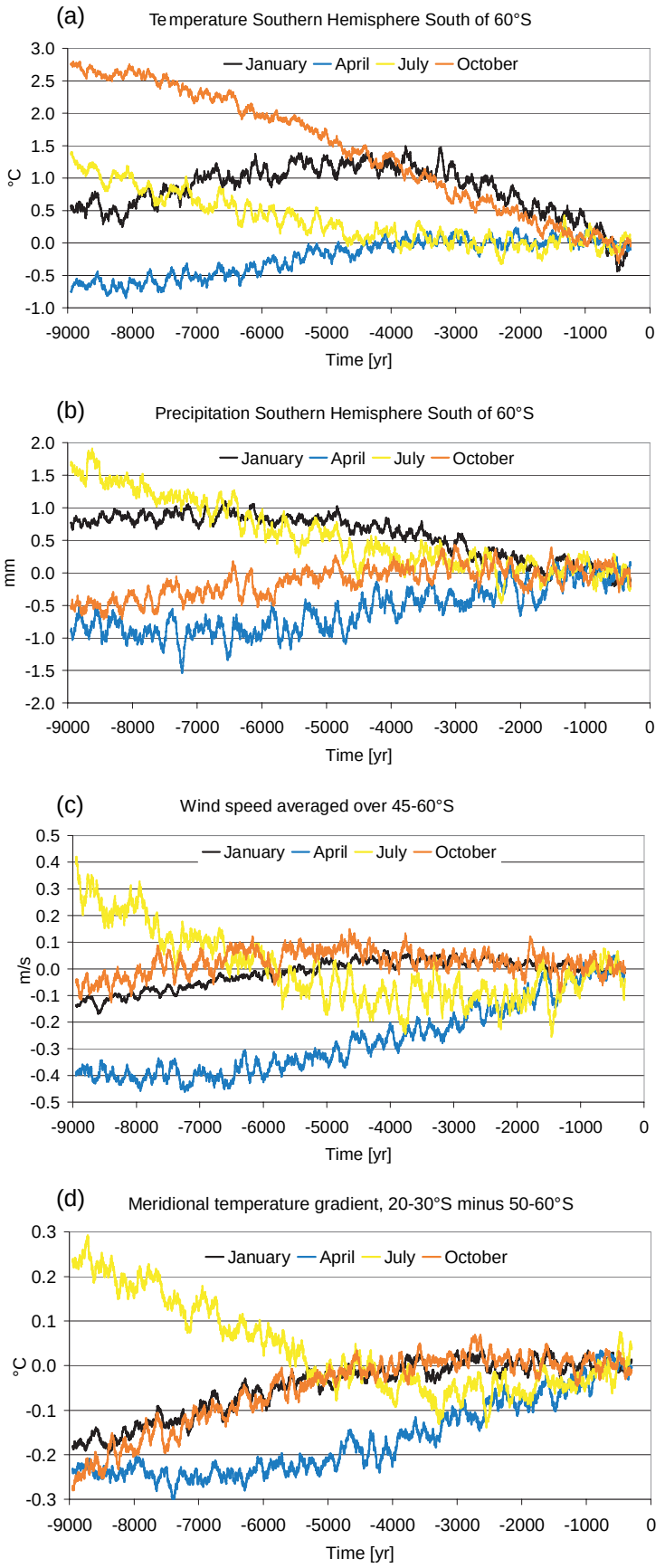

Figure 2 Simulated time series (100-point running means) of (a) monthly surface temperature (°C) averaged over the area South of 60°S, (b) monthly precipitation (mm) averaged over the area South of 60°S, (c) 10-m wind speed (m/s) between 45 and 60°S, and (d) temperature gradient between 20–30°S and 50–60°S (lowest two layers). All curves are shown as deviations from the preindustrial mean (1000–250 yr BP, see Table 1)

Table 1 Absolute surface temperatures and precipitation for the area south of 60°S in four selected time periods: early Holocene (9–7 ka), mid-Holocene (7–4 ka), late Holocene (4–1 ka) and preindustrial (1000–250 yr BP). The monthly standard deviations are also shown

Simulated variable	Time periods			
	9–7 ka	7–4 ka	4–1 ka	preind.
January temperature (°C)	−7.9	−7.4	−7.7	−8.5
Std dev.	1.0	1.0	1.2	1.1
April temperature (°C)	−23.6	−23.2	−22.9	−23.0
Std dev.	0.8	0.8	0.8	0.8
July temperature (°C)	−30.6	−31.1	−31.5	−31.5
Std dev.	0.9	1.0	0.9	1.0
October temperature (°C)	−22.7	−23.4	−24.6	−25.2
Std dev.	0.8	0.9	0.9	0.9
January precipitation (mm)	25.9	25.9	25.4	25.1
Std dev.	0.8	0.8	0.9	0.9
April precipitation (mm)	39.5	39.6	40.1	40.4
Std dev.	1.5	1.5	1.5	1.6
July precipitation (mm)	32.3	31.6	31.1	31.0
Std dev.	1.5	1.4	1.4	1.4
October precipitation (mm)	27.1	27.4	27.5	27.5
Std dev.	1.2	1.3	1.2	1.2

In October, precipitation is enhanced over most places south of 60°S, thus following a trend opposite to that of temperature. This increase during spring is concentrated along the coast of Antarctica (by up to 5 mm, not shown) and is associated with maximum changes in surface pressure (Figure 5). The annual precipitation experiences a small decrease (0.3 mm) from 9 to 0 ka (not shown). It should be noted that the simulated long-term changes in precipitation, as shown in the simulated time series (Figure 2b), are small compared with the interannual variability (as expressed by the standard deviation, Table 1)

Atmospheric circulation

In January and April, the 9 ka surface pressure is 1 to 3 hPa higher over the Southern Ocean than at 0 ka, indicating a less active circumpolar trough in the early part of our simulation (Figure 5). The opposite is seen for July and October, with a deeper circumpolar trough at 9 ka compared with 0 ka (up to 7 hPa difference). The 9 to 0 ka trend in surface pressure is generally consistent with the simulated changes in surface wind speed (Figure 2c). In January and April, the westerlies strengthen from 9 to 0 ka in line with deepening of the circumpolar trough, while in July the westerly winds become weaker towards the end of the experiment in agreement with the 9 to 0 ka increase in surface pressure over the Southern Ocean. Only the response during October is less straightforward, with the wind speed levels averaged over the Southern Ocean staying almost constant during the experiment (Figure 2c), while stronger westerlies would have been expected at 9 ka given the relatively deeper circumpolar trough early in the simulation (Figure 5). However, the October wind speed evolution in Figure 2c is not representative for the entire area south of 45°S, because at 45°S the 9 ka winds were actually stronger than at 0 ka, which is in line with the surface pressure anomalies, while they were weaker at 65°S. The monthly trends in the strength of surface westerlies is associated with the evolution of the meridional temperature gradient (Figure 2d). It should be noted that the differences in wind speed between 9 and 0 ka are small, varying between +3% for July and −4% for April.

The simulated changes in winds and pressure at the surface are also consistent with the simulated evolution of the Antarctic Oscillation (AAO) index, which is defined as the leading principal component of 850 hPa geopotential height anomalies south of 20°S. The AAO is characterized by pressure anomalies of one sign centred on Antarctica and anomalies of the opposite sign centred at about 40–50°S. The AAO index is a measure for the strength of the zonal circulation at SH high latitudes, with higher index values signifying a stronger zonal atmospheric flow. In January and April, the simulated AAO index increases substantially from 9 to 0 ka, while the reverse trends are found for July and October (not shown).

Sea ice

The simulated long-term Holocene response of the sea ice concentration and thickness shows an increase. The evolution of the sea ice cover in March (i.e., at the end of summer) first indicates a slight decrease of 0.3×10^6 km^2 from 9 to 5 ka, after which it increases again by 1×10^6 km^2 to the preindustrial value of 4.7×10^6 km^2 (Figure 6). The March sea ice cover thus experiences the same trend as the summer temperatures. During this season, the overall increase in sea ice is restricted to the western part of the Southern Ocean (Figure 7a and 7c), particularly over the Bellingshausen Sea, where locally a 25-cm increase in thickness is noted (i.e., +40%) together with a 10% increase in cover. In September (end of winter, Figure 6), the sea ice cover follows a linear increase from 9 to 0 ka (by 1.5×10^6 km^2 from 16.2 to 17.7×10^6 km^2). In September the sea ice expands especially in two centers (between 70 and 120°W and around 15°E), which are at the same position as the maximum winter cooling, where the ice concentration increases by up to 20–30% (Figure 7b). The increase in thickness is modest (i.e., between 5 and 15 cm, or about +7%, Figure 7d).

Ocean circulation

The simulated changes in ocean circulation are relatively small. The Antarctic Circumpolar Current is strongest in the early part of the experiment. From 9 to 5 ka, a gradual weakening is noted from 139 to 136 Sv, followed by a slight recovery to 137 Sv (not shown). The amount of Antarctic Bottom Water exported stays more or less stable throughout the experiment, as only a very minor decrease in the first 2 000 years is noted. In addition, the overall strength of the ocean thermohaline circulation, as for instance measured by the export of North Atlantic Deep Water at 20°S, does not change significantly in our experiment (Renssen *et al.*, 2005).

Discussion

Role of local insolation

The temperature evolution from October to May can be explained partly by a delayed response to the local insolation curves of one to two months earlier (i.e., August to March). The overall time lag depends on the thermal inertia of the system. The heat capacity of the oceans is relatively large, leading to a typical lag of two to three months over ocean surfaces, while the thermal inertia is much smaller over continents, resulting in a typical lag of less than one month over land surfaces (e.g., Crucifix *et al.*, 2002). The lag of the temperature averaged over the area south of 60°S compared with insolation is one to two months for October to May. For instance, the January temperatures show a mid-Holocene thermal optimum between 5 and 4 ka that is also present in the insolation curves for November (6 ka) and December (3 ka)

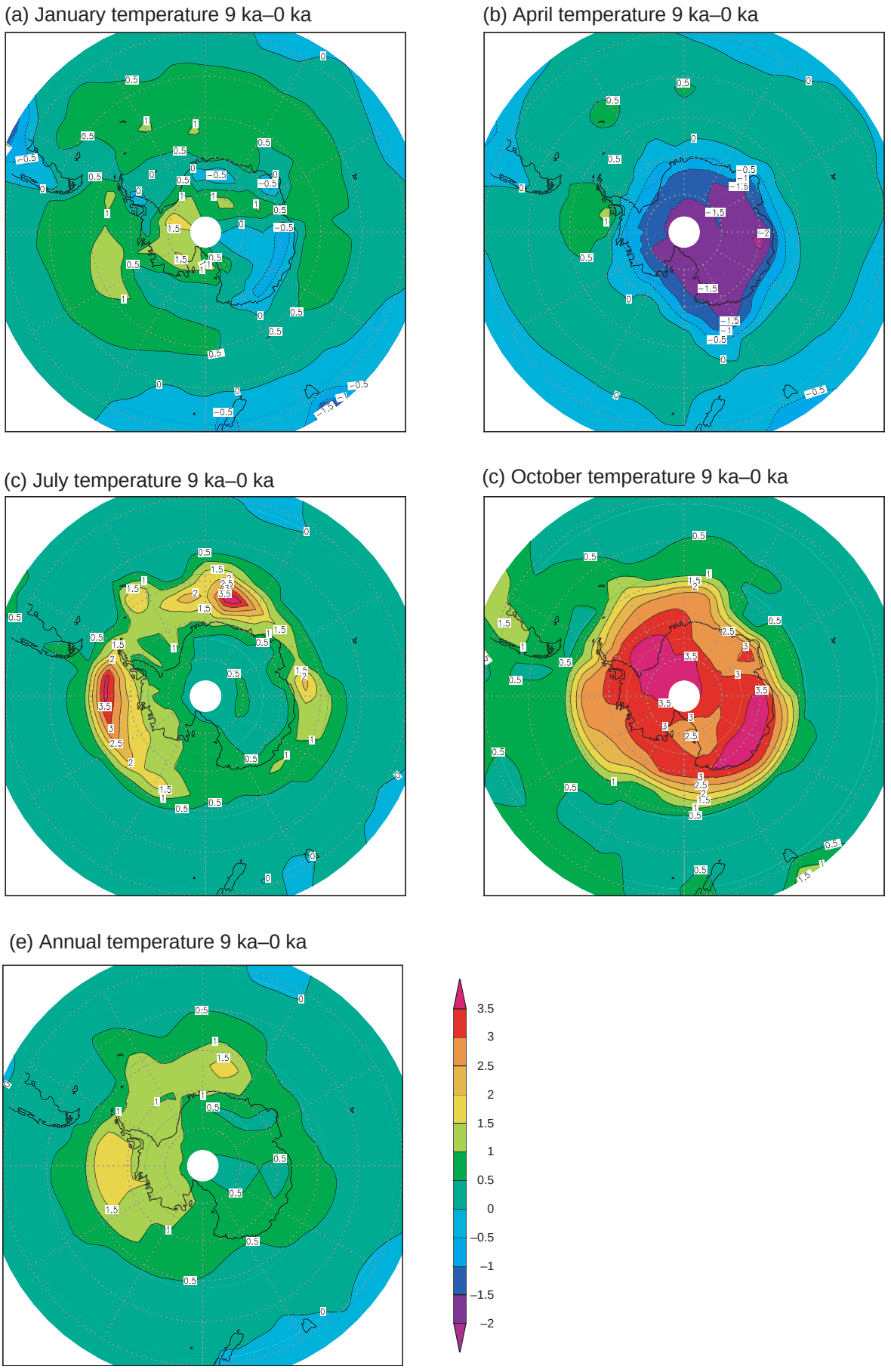

Figure 3 Simulated seasonal 9 ka minus preindustrial change in surface temperature (°C). (a) January, (b) April, (c) July, (d) October, and (e) annual

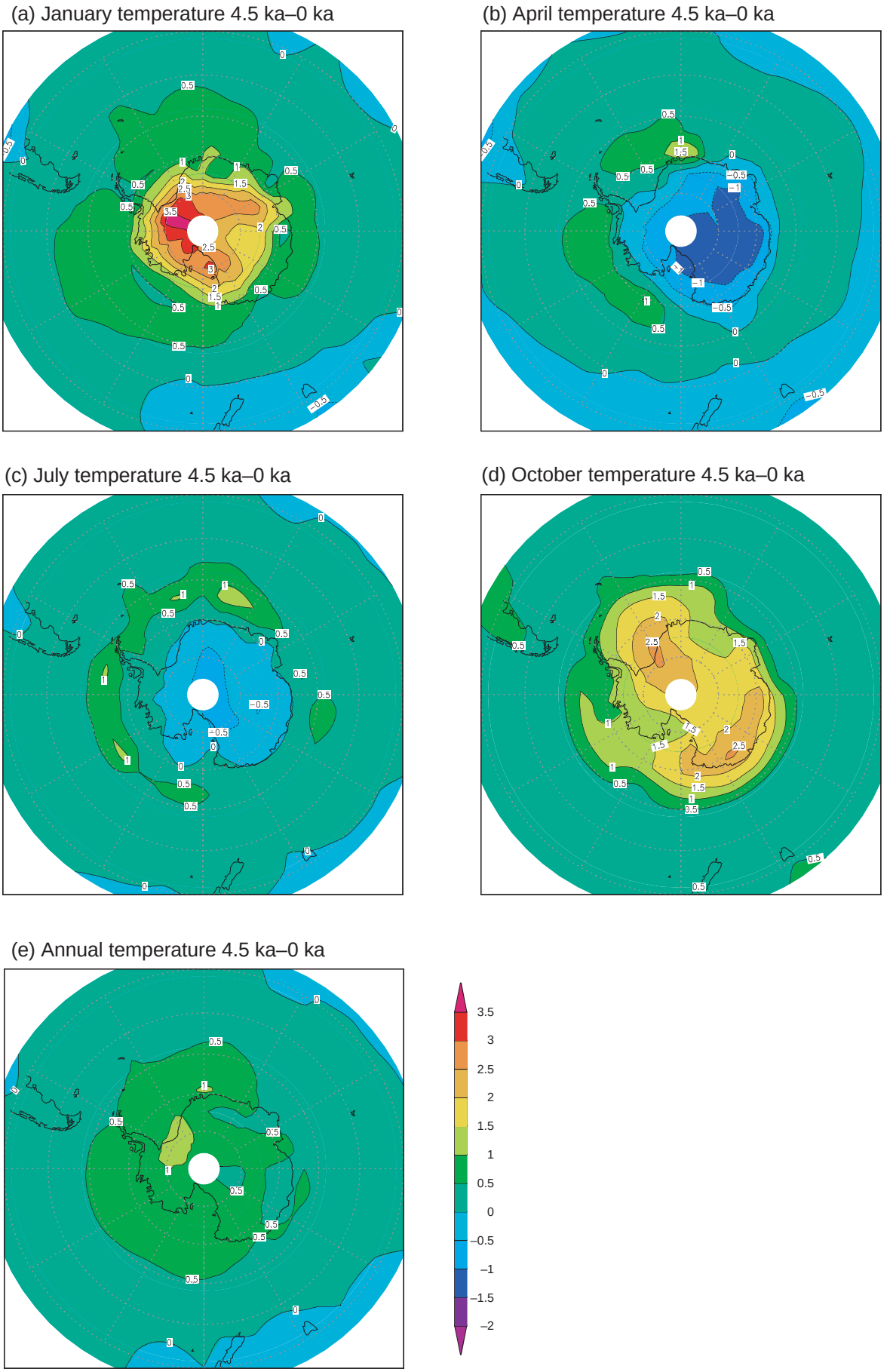

Figure 4 Simulated seasonal 4.5 ka minus preindustrial change in surface temperature (°C). (a) January, (b) April, (c) July, (d) October and (e) annual

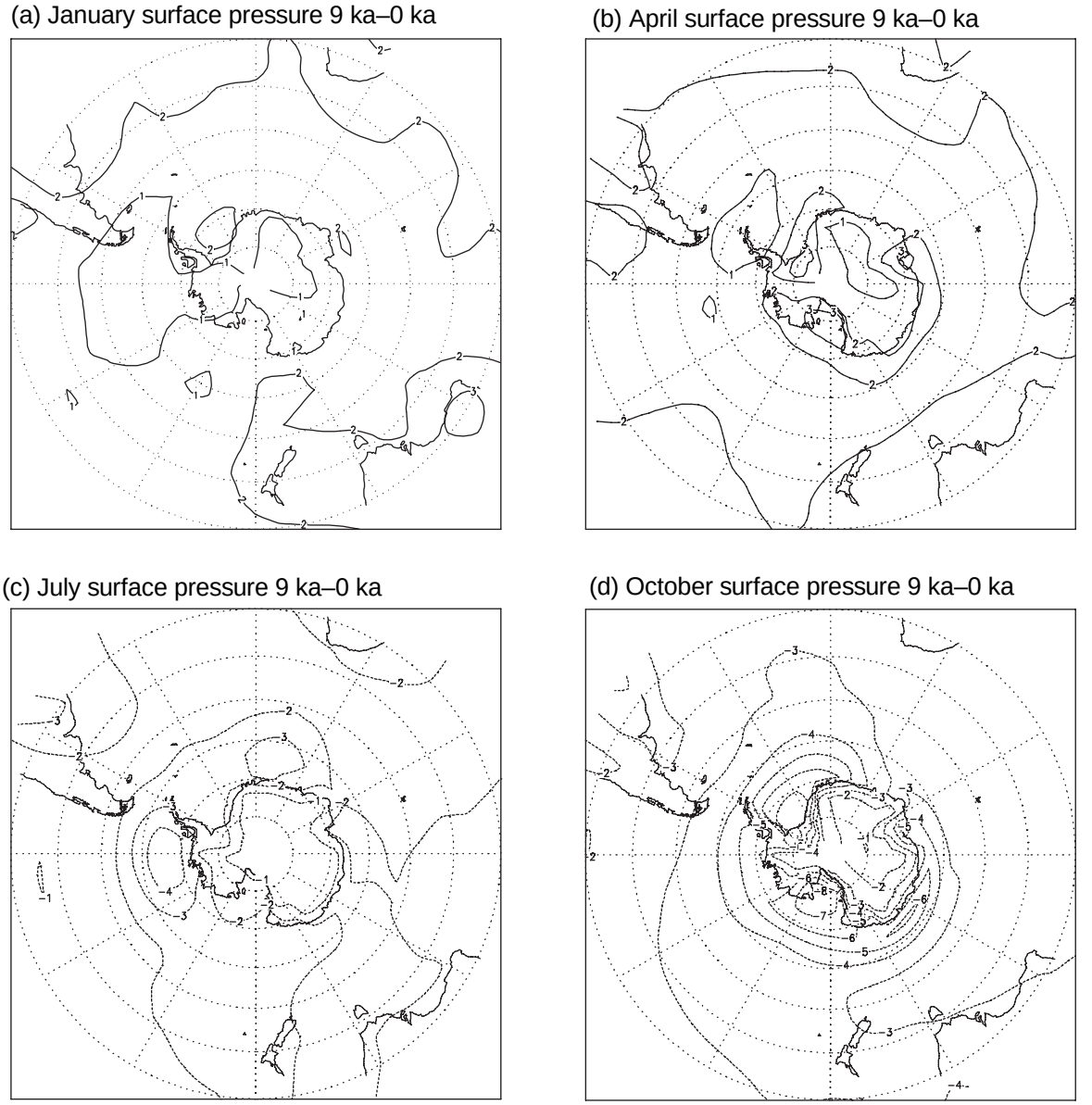

Figure 5 Simulated seasonal 9 ka minus preindustrial change in surface pressure (hPa). (a) January, (b) April, (c) July, (d) October

(compare Figures 1a and 2a). In addition, the relatively warm conditions in October in the early Holocene can be related to the September and August insolation curves. Similarly, the April temperatures are lower than today in the early Holocene, in line with the insolation that is lower than today in February and March. However, even in April, most of the Southern Ocean is warmer in the early Holocene than today, showing that a lagged response to local insolation can provide only part of the explanation. This complexity is also clear for the winter months (June, July, August), as the Holocene insolation for autumn–early winter (April to July) is not changing significantly at SH high latitudes. This implies that the relatively warm early Holocene conditions during winter, as evident in the temperature time series of, for example, July, must originate from other seasons (because of the system memory) or from lower latitudes (because of poleward heat transport).

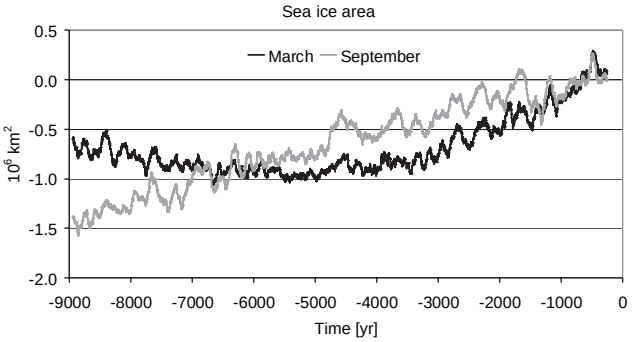

Figure 6 Simulated March (black) and September (grey) time series (100-point running mean) of the sea ice area (10^6 km^2) in the Southern Hemisphere, plotted as deviations from the preindustrial mean (5.4×10^6 km^2 for March, 17.7×10^6 km^2 for September)

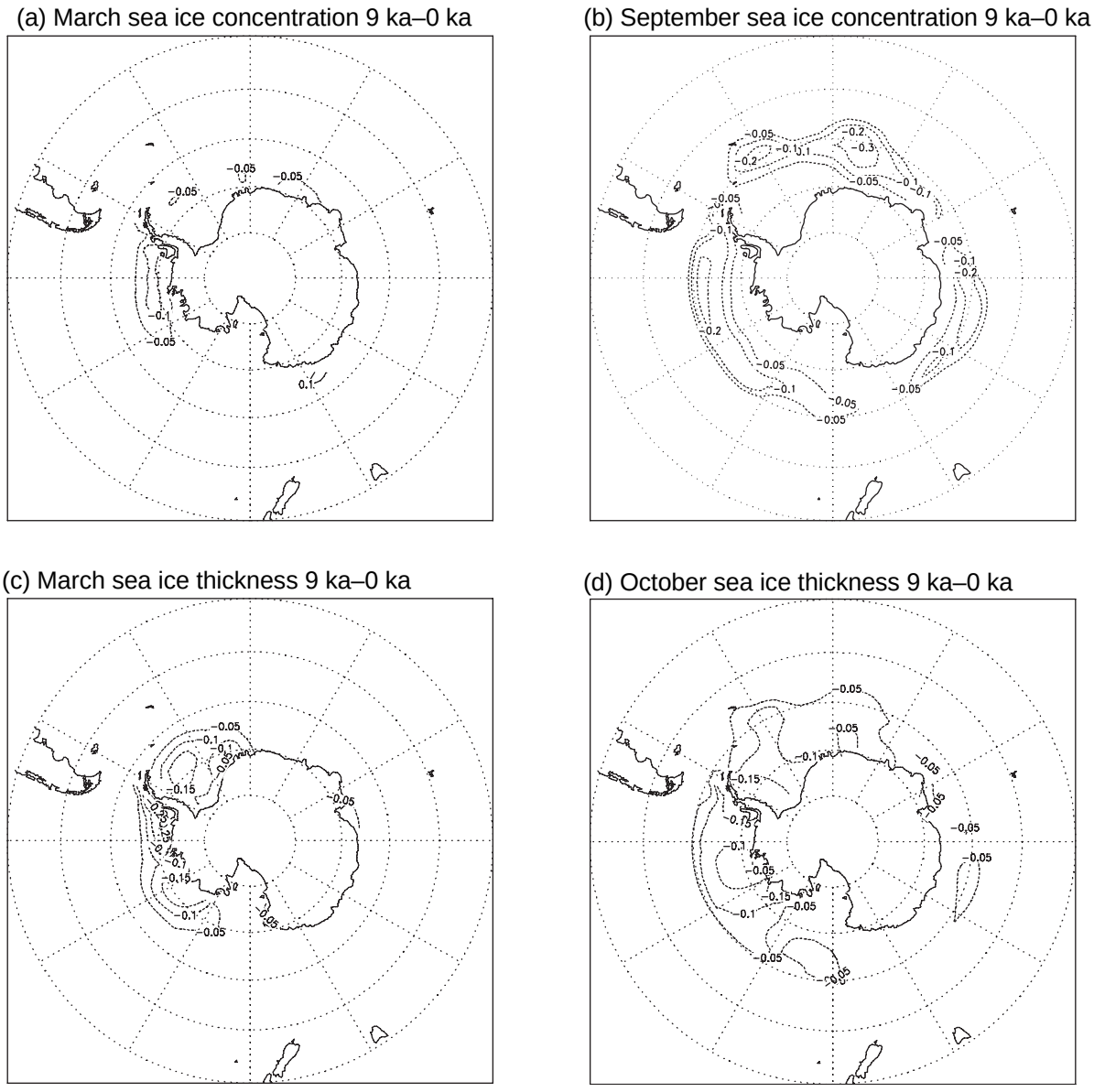

Figure 7 March and September 9 ka minus 0 ka anomalies in sea ice concentration (fraction, upper two graphs) and thickness (in metres, lower two graphs)

Role of the memory of the system

Over the Southern Ocean, the temperature difference compared with 0 ka stays rather constant throughout the year, being always warmer at 9 ka and 4.5 ka than in the late Holocene (Figures 3 and 4), even in seasons during which the surrounding continents are cooler. This suggests that the memory of the system is sufficiently large to smooth seasonal variations related to, e.g., lower insolation during January to March (Figure 1b). In the early Holocene, the relatively high atmospheric temperatures in late winter–early spring (because

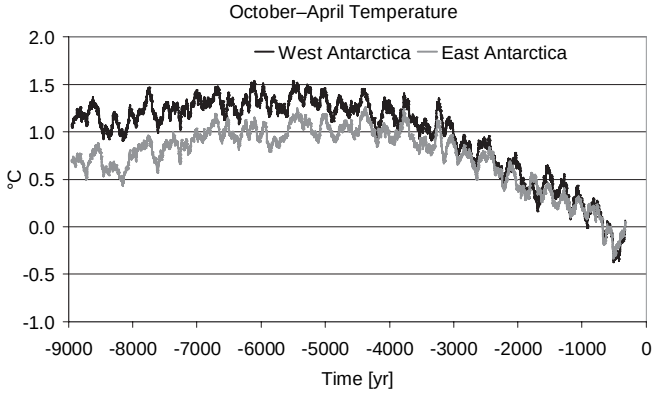

Figure 8 October to April mean temperature evolution for West and East Antarctica (averaged over 65–90°S), plotted as 100-point running average and as deviation from the preindustrial mean (−18.2°C for West Antarctica and −29.7°C for East Antarctica)

of local insolation) lead to warming of the surface ocean (mixed layer) and to relatively thin sea ice and reduced ice cover compared with preindustrial conditions. At this time of year the mixed layer reaches its deepest level. During late spring and summer, the zone situated below the seasonal thermocline (i.e., the winter layer) is no longer in contact with the surface, implying that the warm anomaly is temporarily stored there. The effect of the relatively reduced sea ice conditions is to amplify the already warm conditions in spring because of the ice–albedo and ice–insulation positive feedbacks. The anomalously warm surface conditions are transferred well into the summer, with the Southern Ocean being 1°C warmer at 9 ka in January than at 0 ka (Figure 3a), and the sea ice cover being thinner in March (Figure 7c). In autumn and winter, the mixed layer deepens again, enabling the warm anomaly that is stored under the thermocline to reach the surface. Compared with 0 ka, this results at 9 ka in a relatively strong ocean-to-atmosphere heat flux in July (20–40 W/m^2 at 60°S) and sites with anomalously warm conditions (up to +3.5°C, Figure 3c). Consequently, the relatively warm early Holocene conditions in July can be explained to a large extent by the long memory of the system, as was proposed earlier by Whitlock *et al.* (2001). To summarize, the long memory of the Southern Ocean is due to two different processes, with a surface layer that is responsible for delays of up to three months and a deeper winter layer that is isolated from the surface during part of the year and accounts for the longer timescales. Sea ice plays an important role as an amplifying factor.

Role of long-distance transport

Only the atmosphere plays a role in the changes of poleward heat transport, as the oceanic meridional heat transport does not vary significantly during our experiment. We have shown above that the seasonal evolution of the surface winds (Figure 2c) is closely linked to the trends in the meridional temperature gradient (Figure 2d). In the early Holocene, the meridional temperature gradient was steeper than at 0 ka during July, resulting in relatively strong westerlies, but less steep during April, producing relatively weak westerly winds. In January and October, the differences compared with 0 ka conditions were smaller, but slightly negative. As expected, the meridional temperature gradients for most months are directly associated with the latitudinal insolation gradients of one to two months earlier. Indeed, in the early Holocene the latitudinal insolation gradients were steeper than at 0 ka from May to August (explaining the July temperature gradient), but less steep than 0 ka from September until December (in line with the October and January temperature gradients). Thus, in addition to the local insolation, the distant insolation could also play a role in the Holocene climate evolution at high SH latitudes. An exception is the less steep 9 ka temperature gradient in April (Figure 2d), as this is related to the relatively warm Southern Ocean. In the early Holocene, autumn insolation is reduced compared with 0 ka at all latitudes, resulting in small changes in the latitudinal gradient. However, while this insolation anomaly leads to relatively cool 9 ka conditions at mid and high latitudes, the Southern Ocean is relatively warm because of the long memory of the system, resulting in a relatively weaker meridional temperature gradient in the early Holocene relative to preindustrial conditions. Although the westerlies are related to the poleward heat transport, the simulated 9 to 0 ka changes in the strength of the westerly winds are small (i.e., between +3% for July and −4% for April), indicating that the contribution of the long distance heat transport to the Holocene temperature evolution at SH high latitudes is insignificant compared with the effects of the local insolation and the memory of the system.

Role of greenhouse gas forcing

In addition to orbital forcing, we also prescribed changes in atmospheric CO_2 and CH_4. To evaluate the effect of this greenhouse gas forcing, we performed a second 9 000-yr-long transient experiment that was only forced by the atmospheric concentrations of CO_2 and CH_4 (as shown in Figure 1b). This experiment suggested that over the course of 9 000 years the greenhouse gas forcing is responsible for a gradual warming of 0.5–1.0°C (annual mean) at SH high latitudes. The greenhouse forcing is amplified by progressive melting of sea ice in the Southern Ocean, especially during winter. In other words, at SH high latitudes, the effect of the forcing by atmospheric CO_2 and CH_4 is opposite (long-term warming) to the effect of orbital forcing (long-term cooling). This implies that in our main experiment, in which we combined the two forcings, the orbitally forced overall Holocene cooling is partly counteracted by the greenhouse gas forcing, thus indicating that atmospheric CO_2 and CH_4 have contributed to the configuration of the Holocene climate.

Relevance for proxy-based reconstructions

To what extent are the simulated temperature trends consistent with published proxy records? As noted in the Introduction, proxy data suggest that the timing and characteristics of the period of maximum warmth varied considerably from place to place. Antarctic ice cores provide isotopic evidence for the existence of two thermal optima: one early optimum between 11 and 9 ka and a secondary optimum later in the Holocene (Masson *et al.*, 2000; Masson-Delmotte *et al.*, 2004). As our experiment was started at 9 ka and cannot provide information on the first optimum, we focus here on the timing and nature of the second optimum.

The ice cores show that the second thermal optimum occurred notably earlier in the Ross Sea Sector (7–5 ka) than in Eastern Antarctica (6–3 ka) (Masson *et al.*, 2000), although possibly local effects (e.g., katabatic winds) could have disturbed the isotopic temperature signal. It is difficult to link the isotopic ice-core data to one particular season, as the seasonal distribution of precipitation (i.e., determining the isotopic signal) is not known. However, reconstructions based on biological proxies, which are expected to represent the summer half-year, are generally consistent with the ice-core evidence, also showing that the warm conditions occurred later in Eastern Antarctica than in the western part of the continent (Steig *et al.*, 1998; Domack *et al.*, 2001; Verkulich *et al.*, 2002). For instance, a marine core from the Ross Sea confirms that relatively warm conditions prevailed here between 7 and 5 ka (Steig *et al.*, 1998). Ocean cores from the vicinity of the Antarctic Peninsula even suggest that warm conditions started earlier (i.e., at 9 ka, Domack *et al.*, 2001). Some lacustrine data (i.e., diatoms) from East Antarctica are also consistent with the ice core data, suggesting relatively cool and dry conditions until 6 ka, followed by warmer conditions with a maximum between 4 and 3 ka (Verkulich *et al.*, 2002). However, other diatom-based reconstructions from East Antarctic lakes have been interpreted to show maximum warmth between ~8.5 and ~6 ka, so substantially earlier in the Holocene (Roberts *et al.*, 2004; Wagner *et al.*, 2004).

Marine cores from the Atlantic sector of the Southern Ocean provide quantitative estimates of Holocene climate change, although the accuracy of the radiocarbon chronologies is restricted by the lack of knowledge of the local marine reservoir age. A diatom-based reconstruction from an ocean

core at 50°S (Nielsen *et al*., 2004) suggests early in the Holocene (until 6.2 ka) summer SSTs 1–2°C above the long-term mean and little sea ice (presence during less than 1 month/yr). This relatively warm phase is followed by cool conditions between 6.2 and 2.9 ka, with summer SSTs of 1°C below the long-term average and ice presence during more than 1 month/yr. According to the reconstructions from this core, the late Holocene (after 2.9 ka) was again characterized by relatively warm conditions. A diatom record from a nearby core (53°S) suggests a similar Holocene climate evolution, with a cooling of ~2°C around 5.5 ka (February SST), followed by warmer conditions in the late Holocene (Hodell *et al*., 2001). In these studies, the evolution during the first half of the Holocene is explained by a response to Northern Hemisphere insolation (at 60°N), involving a weakening of the thermohaline circulation, leading to reduced northward heat transport by the Atlantic Ocean and accumulation of heat in the Southern Ocean. The warming during the late Holocene has been linked to local summer insolation at SH high latitudes (Nielsen *et al*., 2004).

When comparing the proxy-based reconstructions with our model results it is important to establish what season the proxies really represent, since our simulation suggests that the temperature evolution differs substantially from season to season. The simulated summer temperatures experience a thermal maximum between 6 and 3 ka, while the spring temperature is highest at 9 ka and the autumn temperature peaks at 0 ka (Figure 2a). Consequently, part of the variations in the timing of the maximum warmth seen between reconstructions could be related to differences in the seasonal dependence of the proxies. For example, reconstructions based on diatom species that bloom in spring are likely to show an earlier thermal optimum than one based on species that bloom in mid-summer.

Even when this seasonal dependence of proxies is left out of consideration, our model results appear to be consistent with the reconstructions. The simulated temperature evolution for the summer half year (October to April) suggests that the peak of the thermal optimum was 2000 to 1000 years earlier in West Antarctica (7–5 ka) than in East Antarctica (5.5–4 ka; Figure 8). In our model, this difference is caused by the relatively strong reduction of sea ice in the early Holocene in the western sector of the Southern Ocean relative to the eastern sector (Figure 7a–d). This resulted in relatively high early Holocene temperatures in western Antarctica compared with the eastern part of the continent.

Our results suggest that the long-term Holocene climate evolution at SH high latitudes can be explained by the combined effects of local orbital forcing and the long memory of the system. However, some aspects of the Holocene climate have not been reproduced in our experiment, such as the small summer warming during the late Holocene reconstructed in the Atlantic sector (Hodell *et al*., 2001; Nielsen *et al*., 2004). Nevertheless, for the period after 9 ka, it appears that there is no need to invoke Northern Hemisphere insolation and teleconnections with North Atlantic climate, as was proposed in some recent studies (Hodell *et al*., 2001; Nielsen *et al*., 2004).

Conclusions

We have performed a 9000-yr-long transient simulation with a coupled climate model to study the response to orbital and greenhouse gas forcing of the SH high-latitude climate. Our results suggest the following.

(1) The simulated long-term Holocene temperature evolution varied substantially from season to season. In summer, a thermal maximum was reached between 6 and 3 ka, with temperatures locally 3°C above the preindustrial mean in West Antarctica. The autumn temperature experienced a long-term increase, particularly in the first half of the Holocene, where a 1.5°C warming was found over the Antarctic continent. In winter, conditions over the Southern Ocean were relatively warm in the early Holocene (up to 3.5°C warmer than at 0 ka), followed by a gradual cooling. The spring temperatures were strongly reduced during the course of the Holocene, as they were more than 3°C above the preindustrial level at 9 ka. Over the Southern Ocean, the early and mid-Holocene temperatures were higher than the 0 ka climate in all seasons. The seasonal evolution of precipitation and sea ice was generally similar to the temperature trends.

(2) The temperature trends can be explained by a combination of two factors: (i) local orbital forcing, as temperature trends were generally showing a one to two month lag to local insolation, and (ii) the long memory of the system, producing year-round warm conditions in the Southern Ocean. The system's long memory is related to the large heat capacity of the Southern Ocean and the effect of two layers: a surface layer including sea ice, responsible for lags of up to three months, and a deeper level, below the summer mixed layer, in which seasonal thermal anomalies are stored, responsible for the longer-term lags. Sea ice acts as a strong amplifying factor through the positive ice–albedo and ice–insulation feedbacks. Greenhouse gas forcing had a weaker, but opposite, effect (long-term warming) compared with the orbital forcing (long-term cooling).

(3) The simulation suggests that, compared with the preindustrial situation, the early Holocene sea-ice cover was more reduced in the western sector of the Southern Ocean than in the eastern sector, leading to annually persistent differences in 9–0 ka temperature anomalies between the west Antarctica (warmer) and east Antarctica (cooler). As a result, the thermal maximum occurred a few thousand years later in the eastern part of the continent, which has also been observed in ice cores and other palaeoclimatic data.

(4) Our results suggest that long-term Holocene temperature trends can, to a large extent, be explained by a response to insolation variations in the Southern Hemisphere, implying that teleconnections to the Northern Hemisphere appear not to be necessary to explain the first order response of the Southern Ocean during the last 9000 years of the Holocene.

Acknowledgements

The comments of J. Lowe, V. Markgraf and an anonymous referee are gratefully acknowledged. HR is supported by the Netherlands Organization for Scientific Research (NWO). HG is Research Associate at the Belgian National Fund for Scientific Research. This study was carried out as part of the Belgian Second Multiannual Scientific Support Plan for a Sustainable Development Policy (Belgian Federal Science Policy Office, contract EV/10/9A and EV/10/7D) and the European Research Programme on Environment and Sustainable Development (European Commission, contract EVK2-2001-00263). VMD is supported by the French Programme National d'Etude du Climat (PNEDC/IMPAIRS). V. Brovkin (Potsdam Institute for Climate Impact Research) kindly made VECODE available for this study. J.M. Campin (MIT) is thanked for programming the coupling of VECODE to ECBilt

and for model testing. This manuscript benefited from discussions with M.F. Loutre (UCL, Louvain-la-Neuve).

References

Berger, A.L. 1978: Long-term variations of daily insolation and Quaternary climatic changes. *Journal of the Atmospheric Sciences* 35, 2363–67.

Brachfeld, S., Domack, E., Kissel, C., Laj, C., Leventer, A., Ishman, S., Gilbert, R., Camerlenghi, A. and **Eglinton, L.B.** 2003: Holocene history of the Larsen-A Ice Shelf constrained by geomagnetic paleointensity dating. *Geology* 31, 749–52.

Brovkin, V., Bendtsen, J., Claussen, M., Ganopolski, A., Kubatzki, C., Petoukhov, V. and **Andreev, A.** 2002: Carbon cycle, vegetation and climate dynamics in the Holocene: experiments with the CLIMBER-2 model. *Global Biogeochemical Cycles* 16, 1139, DOI: 10.1029/2001GB001662.

Campin, J.-M. and **Goosse, H.** 1999: Parameterization of density-driven downsloping flow for a coarse-resolution ocean model in z-coordinate. *Tellus* 51A, 412–30.

Crucifix, M., Loutre, M.F., Tulkens, P., Fichefet, T. and **Berger, A.** 2002: Climate evolution during the Holocene: a study with an Earth system model of intermediate complexity. *Climate Dynamics* 19, 43–60.

Cubasch, U., Meehl, G.A., Boer, G.J., Stouffer, R.J., Dix, M., Noda, A., Senior, C.A., Raper, S. and **Yap, K.S.** 2001: Projections of future climate change. In Houghton, J.T., Ding, Y., Griggs, D.J., Noguer, M., van der Linden, P.J., Dai, X., Maskell, K. and Johnson, C.A., editors, *Climate change 2001: the scientific basis. Contribution of working group I to the third assessment report of the Intergovernmental Panel on Climate Change*. Cambridge and New York: Cambridge University Press, 525–82.

Domack, E., Leventer, A., Dunbar, R., Taylor, F., Brachfeld, S., Sjunnekog, C. and **Party, O.L.S.** 2001: Chronology of the Palmer Deep site, Antarctic Peninsula: a Holocene palaeoenvironmental reference for the circum-Antarctic. *The Holocene* 11, 1–9.

Folland, C.K., Karl, T.R., Christy, R.A., Clarke, R.A., Gruza, G.V., Jouzel, J., Oerlemans, J., Salinger, M.J. and **Wang, S.-W.** 2001: Observed climate variability and change. In Houghton, J.T., Ding, Y., Griggs, D.J., Noguer, M., van der Linden, P.J., Dai, X., Maskell, K. and Johnson, C.A., editors, *Climate change 2001: the scientific basis. Contribution of working group I to the third assessment report of the Intergovernmental Panel on Climate Change*. Cambridge and New York: Cambridge University Press, 99–181.

Gent, P.R. and **McWilliams, J.C.** 1990: Isopycnal mixing in ocean general circulation models. *Journal of Physical Oceanography* 20, 150–55.

Goosse, H. and **Fichefet, T.** 1999: Importance of ice–ocean interactions for the global ocean circulation: a model study. *Journal of Geophysical Research* 104, 23 337–55.

Goosse, H. and **Renssen, H.** 2001: A two-phase response of the Southern Ocean to an increase in greenhouse gas concentrations. *Geophysical Research Letters* 28, 3469–72.

—— 2004: Exciting natural modes of variability by solar and volcanic forcing: idealized and realistic experiments. *Climate Dynamics* 23, 153–63.

—— 2005: Simulating the evolution of ice cover in the Southern Ocean since 1750 AD: implications of the long memory of the ocean. *International Journal of Climatology* 25, 569–79.

Goosse, H., Deleersnijder, E., Fichefet, T. and **England, M.** 1999: Sensitivity of a global ocean–sea ice model to the parameterization of vertical mixing. *Journal of Geophysical Research* 104, 13 681–95.

Goosse, H., Selten, F.M., Haarsma, R.J. and **Opsteegh, J.D.** 2001: Decadal variability in high northern latitudes as simulated by an intermediate-complexity climate model. *Annals of Glaciology* 33, 525–32.

—— 2002: A mechanism of decadal variability of the sea-ice volume of the Northern Hemisphere. *Climate Dynamics* 19, 61–83.

—— 2003: Large sea-ice volume anomalies simulated in a coupled climate model. *Climate Dynamics* 20, 523–36.

Goosse, H., Masson-Delmotte, V., Renssen, H., Delmotte, M., Fichefet, T., Morgan, V., van Ommen, T., Khim, B.K. and **Stenni, B.** 2004: A late medieval warm period in the Southern Ocean as a delayed response to external forcing? *Geophysical Research Letters* 31, L06203, DOI: 10.1029/019140.

Hewitt, C.D. and **Mitchell, J.F.B.** 1998: A fully coupled GCM simulation of the climate of the mid-Holocene. *Geophysical Research Letters* 25, 361–64.

Hodell, D.A., Kanfoush, S.L., Shemesh, A., Crosta, X., Charles, C.D. and **Guilderson, T.P.** 2001: Abrupt cooling of Antarctic surface waters and sea ice expansion in the South Atlantic sector of the Southern Ocean at 5000 cal yr BP. *Quaternary Research* 56, 191–98.

Jacobsen, S.S. and **Comiso, J.C.** 1997: Climate variability in the Amundsen and Bellingshausen Seas. *Journal of Climate* 10, 697–709.

Joussaume, S. and **Braconnot, P.** 1997: Sensitivity of paleoclimate simulation results to season definitions. *Journal of Geophysical Research* 102, 1943–56.

Knutti, R., Flückiger, J., Stocker, T.F. and **Timmermann, A.** 2004: Strong hemispheric coupling of glacial climate through freshwater discharge and ocean circulation. *Nature* 430, 851–56.

Lamy, F., Rühlemann, C., Hebbeln, D. and **Wefer, G.** 2002: High- and low-latitude climate control on the position of the southern Peru–Chile current during the Holocene. *Paleoceanography* 17, 1028, DOI: 10.1029/2001PA000727.

Masson, V., Vimeux, F., Jouzel, J., Morgan, V., Delmotte, M., Ciais, P., Hammer, C., Johnsen, S., Lipenkov, V.Y., Mosley-Thompson, E., Petit, J.-R., Steig, E.J., Stievenaud, M. and **Vaikmae, R.** 2000: Holocene climate variability in Antarctica based on 11 ice-core isotopic records. *Quaternary Research* 54, 348–58.

Masson-Delmotte, V., Stenni, B. and **Jouzel, J.** 2004: Common millennial-scale variability of Antarctic and Southern Ocean temperatures during the past 5000 years reconstructed from the EPICA Dome C ice core. *The Holocene* 14, 145–51.

Mellor, G.L. and **Yamada, T.** 1982: Development of a turbulence closure model for geophysical fluid problems. *Review of Geophysics and Space Physics* 20, 851–75.

Nielsen, S.H.H., Koç, N. and **Crosta, X.** 2004: Holocene climate in the Atlantic sector of the Southern Ocean: controlled by insolation or oceanic circulation? *Geology* 32, 317–20.

Opsteegh, J.D., Haarsma, R.J., Selten, F.M. and **Kattenberg, A.** 1998: ECBILT: a dynamic alternative to mixed boundary conditions in ocean models. *Tellus* 50A, 348–67.

Raynaud, D., Barnola, J.-M., Chappellaz, J., Blunier, T., Indermühle, A. and **Stauffer, B.** 2000: The ice record of greenhouse gases: a view in the context of future changes. *Quaternary Science Reviews* 19, 9–17.

Renssen, H., Goosse, H., Fichefet, T. and **Campin, J.-M.** 2001: The 8.2 kyr BP event simulated by a global atmosphere–sea-ice–ocean model. *Geophysical Research Letters* 28, 1567–70.

Renssen, H., Goosse, H. and **Fichefet, T.** 2002: Modeling the effect of freshwater pulses on the early Holocene climate: the influence of high frequency climate variability. *Paleoceanography* 17, 1020, DOI 10.1029/2001PA000649.

Renssen, H., Brovkin, V., Fichefet, T. and **Goosse, H.** 2003a: Holocene climate instability during the termination of the African Humid Period. *Geophysical Research Letters* 30, 1184, DOI: 10.1029/2002GL016636.

Renssen, H., Goosse, H. and **Fichefet, T.** 2003b: On the non-linear response of the ocean thermohaline circulation to global deforestation. *Geophysical Research Letters* 30, 1061, DOI: 10.1029/2002GL016155.

Renssen, H., Goosse, H., Fichefet, T., Brovkin, V., Driesschaert, E. and **Wolk, F.** 2005: Simulating the Holocene climate evolution at northern high latitudes using a coupled atmosphere–sea ice–ocean–vegetation model. *Climate Dynamics* 24, 23–43.

Roberts, D., McMinn, A., Cremer, H., Gore, D.B. and **Melles, M.** 2004: The Holocene evolution and palaeosalinity history of Beall Lake, Windmill Islands (East Antarctica) using an expanded

diatom-based weighted averaging model. *Palaeogeography, Palaeoclimatology, Palaeoecology* 208, 121–40.

Rossow, W.B., Walker, A.W., Beuschel, D.E. and **Roiter, M.D.** 1996: *International satellite cloud climatology project (ISCCP) documentation of new cloud datasets*. Geneva: World Meteorological Organisation, WMO/TD-No 737.

Schaeffer, M., Selten F.M., Opsteegh, J.D. and **Goosse, H.** 2002: Intrinsic limits to predictability of abrupt regional climate change in IPCC SRES scenarios. *Geophysical Research Letters* 29, 1767, DOI: 10.1029/2002GL015254.

Stammerjohn, S.E. and **Smith, R.C.** 1997: Opposing Southern Ocean climate patterns as revealed by trends in regional sea ice coverage. *Climatic Change* 37, 617–39.

Steig, E.J., Hart, C.P., White, W.J.C., Cunningham, W.L., Davis, M.D. and **Saltzman, E.S.** 1998: Changes in climate ocean and ice-sheet conditions in the Ross Embayment, Antarctica, at 6 ka. *Annals of Glaciology* 27, 305–10.

Thompson, D.W.J. and **Solomon, S.** 2002: Interpretation of recent Southern Hemisphere climate change. *Science* 296, 895–99.

Vaughan, D.G., Marshall, G.J., Connolley, W.M., King, J.C. and **Mulvaney, R.** 2001: Devil in the detail. *Science* 293, 1777–79.

Verkulich, S.R., Melles, M., Hubberten, H.W. and **Pushina, Z.V.** 2002: Holocene environmental changes and development of Figurnoye Lake in the southern Bunger Hills, East Antarctica. *Journal of Paleolimnology* 28, 253–67.

Vimeux, E., Masson, V., Jouzel, J., Petit, J.R., Steig, E.J., Stievenard, M., Vaikmae, R. and **White, J.W.C.** 2001: Holocene hydrological cycle changes in the Southern Hemisphere documented in East Antarctic deuterium excess records. *Climate Dynamics* 17, 503–13.

Wagner, B., Cremer, H., Hultzsch, N., Gore, D.B. and **Melles, M.** 2004: Late Pleistocene and Holocene history of Lake Terrasovoje, Amery Oasis, East Antarctica, and its climatic and environmental implications. *Journal of Paleolimnology* 32, 321–39.

Wang, Y., Mysak, L., Wang, Z. and **Brovkin, V.** 2005: The greening of the McGill Paleoclimate model. Part II: Millennial-scale climate changes. *Climate Dynamics* 24, 481–96.

Weber, S.L. 2001: The impact of orbital forcing on the climate of an intermediate-complexity coupled model. *Global and Planetary Change* 30, 7–12.

Weber, S.L., Crowley, T.J. and **van der Schrier, G.** 2004: Solar irradiance forcing of centennial climate variability during the Holocene. *Climate Dynamics* 24, 539–53.

Whitlock, C., Bartlein, P.J., Markgraf, V. and **Ashworth, A.C.** 2001: The Midlatitudes of North and South America during the last glacial maximum and early Holocene: similar paleoclimatic sequences despite differing large-scale controls. In Markgraf, V., editor, *Interhemispheric climate linkages*. San Diego CA: Academic Press, 391–416.